Fracture of Sub-20nm Ultrathin Gold Nanowires

*Yang Lu, Jun Song, Jian Yu Huang, and Jun Lou**

Fracture of metals at the nanoscale and corresponding failure mechanisms have recently attracted considerable interest. However, quantitative in situ fracture experiments of nanoscale metals are rarely reported. Here it is shown that, under uni-axial tensile loading, single crystalline ultrathin gold nanowires may fracture in two modes, displaying distinctively different fracture morphologies and ductility. In situ high resolution transmission electron microscopy (HRTEM) studies suggest that the unexpected brittle-like fracture was closely related to the observed twin structures, which is very different from surface dislocation nucleation/propagation mediated mechanism in ductile fracture mode. Molecular dynamics (MD) simulations further reveal the processes of shear-induced twin formation and damage initiation at the twin structure/free surface interface, confirming the experimentally observed differences in fracture morphology and ductility. Finally, a fracture criterion based on competition between twin formation and surface dislocation nucleation/propagation as a function of misalignment angle is discussed.

1. Introduction

As the critical feature sizes of modern electronic devices continue to shrink, extensive research has been focused on the development and implementation of next-generation interconnects in order to incorporate increasingly small feature sizes with high performance and reliability in a cost-effective manner. While current lithography may encounter a barrier when the critical dimension approaches sub-20nm,[1] ultrathin metallic nanowires,[2] such as gold,[3–6] silver,[7–9] telluiurm,[10,11] palladium,[11,12] and platinum,[11–13] nanowires with diameter less than 15 nm, have been recently fabricated via bottom-up methods and may potentially satisfy the stringent nanoelectronic device requirements. Ultrathin gold nanowire is particularly promising candidate for future interconnects and as an active component in nanoscale electric and mechanical devices,[3,14] owing to its excellent electrical and mechanical properties and desired chemical inertness. However, full realization of ultrathin gold nanowires' potential in nanoscale electrical and mechanical devices requires a comprehensive reliability study of their fracture behaviours and corresponding mechanisms, which is yet to be explored.

In the past decades, significant progresses have been made in quantitatively measuring mechanical properties of metallic nanostructures (e.g., nanowires,[15–20] nano pillars,[21–25] atom chains)[26–28] However, quantitative understanding of sub-20 nm metallic nanowire fracture behaviours, which requires direct correlations between mechanical measurements and corresponding substructure evolutions, remains elusive. The preferred uni-axial tensile fracture experiments for high aspect ratio ultrathin nanowire samples remains quite challenging for these exceedingly small samples due to sample handling and clamping issues. Typical clamping methods involving focus ion beam (FIB) deposition may introduce significant surface contamination,[29] and local heat-induced spot welding could potentially damage the initial sample structures and morphologies.[30–32] Using recently developed cold welding techniques for ultrathin gold nanowires,[33] we manage to overcome these difficulties and are now able to perform robust individual nanowire picking-up and clamping procedures repeatedly (see Experimental Section and Supporting Information), allowing systematic study of tensile fracture behaviours for sub-20 nm gold nanowires.

Quantitative transmission electron microscopy (TEM) tensile experiments of 22 sub-20 nm <111> gold nanowires were successfully carried out using a Nanofactory in situ TEM-AFM (atomic force microscopy) sample holder (see Supporting Information), in which a silicon AFM cantilever with known spring constant acts as the force sensor and a gold scanning tunneling microscopy (STM) probe driven by a piezo manipulator acts as the actuator. The nanowire samples were clamped between the gold STM probe and the silicon AFM cantilever through in situ nanomanipulation and cold-welding assisted sample clamping.[33] The force and displacement data with high precision and sampling rates were directly recorded by an integrated MEMS-based sensor[34] (see Experimental Section).

2. Results

Figure 1 shows a typical tensile test of a <111> ultrathin gold nanowire sample (~7.5 nm in diameter and ~114 nm in length)

Dr. Y. Lu, Prof. J. Lou
Department of Mechanical Engineering and Materials Science
Rice University
Houston, TX 77005
E-mail: jlou@rice.edu
Prof. J. Song
Division of Engineering
Brown University
Providence, RI 02912, USA
J. Y. Huang
Center for Integrated Nanotechnologies (CINT)
Sandia National Laboratories
Albuquerque, NM 87185, USA

DOI: 10.1002/adfm.201101224

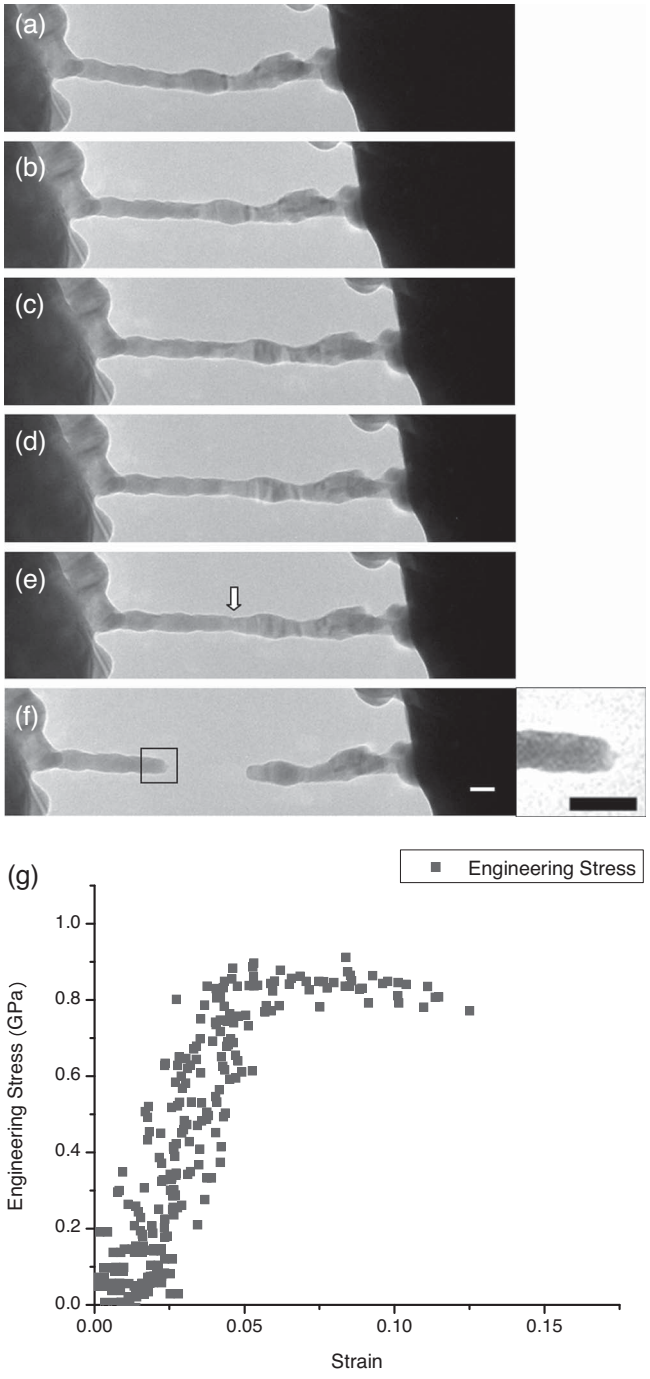

Figure 1. A typical in situ tensile test of a long ultrathin gold nanowire fractured in ductile mode: a) nanowire at the initial relaxed state; b) nanowire under initial loading; c–e) nanowire underwent plastic deformation, thinning and necking process; f) final fracture stage, left side of the sample returned to no-force state along with the AFM cantilever (insert showing the magnified view of the fracture surface, both scale bars 10 nm); g) the corresponding engineering stress-strain curve.

prepared by nanomanipulation and cold welding processes. The nanowire was stretched toward the right side by the STM probe at a constant displacement rate of ~0.3 nm/s. This particular sample experienced extensive plastic deformation (Figure 1c–e) and formed a neck (Figure 1e, as indicated by the white arrow) in the middle section before final fracture. In Figure 1f, the fracture surface of the left part of the nanowire formed a sharp tip when imaged at higher resolution. The corresponding stress versus strain curve was plotted in Figure 1g. A distinct yielding point at engineering stress of ~900 MPa and strain of ~5% was observed, and this sample experienced a total 12.4% engineering strain before final fracture. The engineering fracture strength was subsequently determined to be ~774 MPa. Due to the relatively low magnification (needed for video calibration) and low video recording speed (0.5 frame per second) used in this in situ experiments, we were not able to capture the instantaneous diameter just before the final facture. Nonetheless, by measuring the diameter at the necking section (i.e., ~3.5 nm) using the last frame prior to fracture, we obtained a nominal true breaking stress of ~3.55 GPa (considering the actual instantaneous diameter should be less than 3.5 nm, the actual true fracture strength may even be higher).

Interestingly, this "typical" elasto-plastic ductile facture was not always observed in our systematic investigations. In **Figure 2**, another tensile test with distinctively different fracture behavior, i.e., brittle-like fracture was observed. The sample experienced comparatively much shorter elongation and suddenly fractured, leaving a relatively flat fracture surface (Figure 2b). For this particular sample, the diameter was also ~7.5 nm and the initial length was ~60.5 nm. At the beginning stage of the tensile test, the load was applied along the nanowire axis with a misalignment angle of ~25°, due to the changes in sample position and orientation during clamping process. It should be noted that even though the initial misalignment angle seemed to be large, much better alignment were typically achieved during course of actual tensile testing. Corresponding stress–strain curves in Figure 2c showed that engineering stress of the sample continuously increased up to ~1 GPa before final fracture at ~5% engineering strain. No apparent yielding and necking was observed.

By carefully examining the fracture morphologies, stress–strain curves, and deformation processes from the videos of all 22 successful in situ quantitative tensile experiments performed on sub-20 nm Au nanowires, we were able to distinguish the "ductile" versus "brittle-like" fracture modes and divide all the tests into two categories as summarized in **Table 1** using the three criteria defined in **Table 2**. It might be noted that the "ductility" (breaking strain) calculated here was engineering strain, in which the whole length of the original nanowire was considered. Due to the fact that the plastic deformation of ultrathin nanowires was pretty localized (i.e., the onset of plastic deformation, thinning, necking and final breaking would only occur within a small portion of the long nanowire), the actual localized plastic strain for ductile fracture cases could be much higher. These had been verified in our experiments by selecting a section with apparent necking and a ~90% local breaking strain was obtained in the ductile fracture case as shown in Figure 1. In addition, while the ductility (breaking strain) was generally used as the primary criterion, fracture surface morphology and deformation process observed from the videos were often more straightforward in determining the fracture modes without the need of labor-intensive data processing and extraction. However, due to rearrangements of surface atoms,

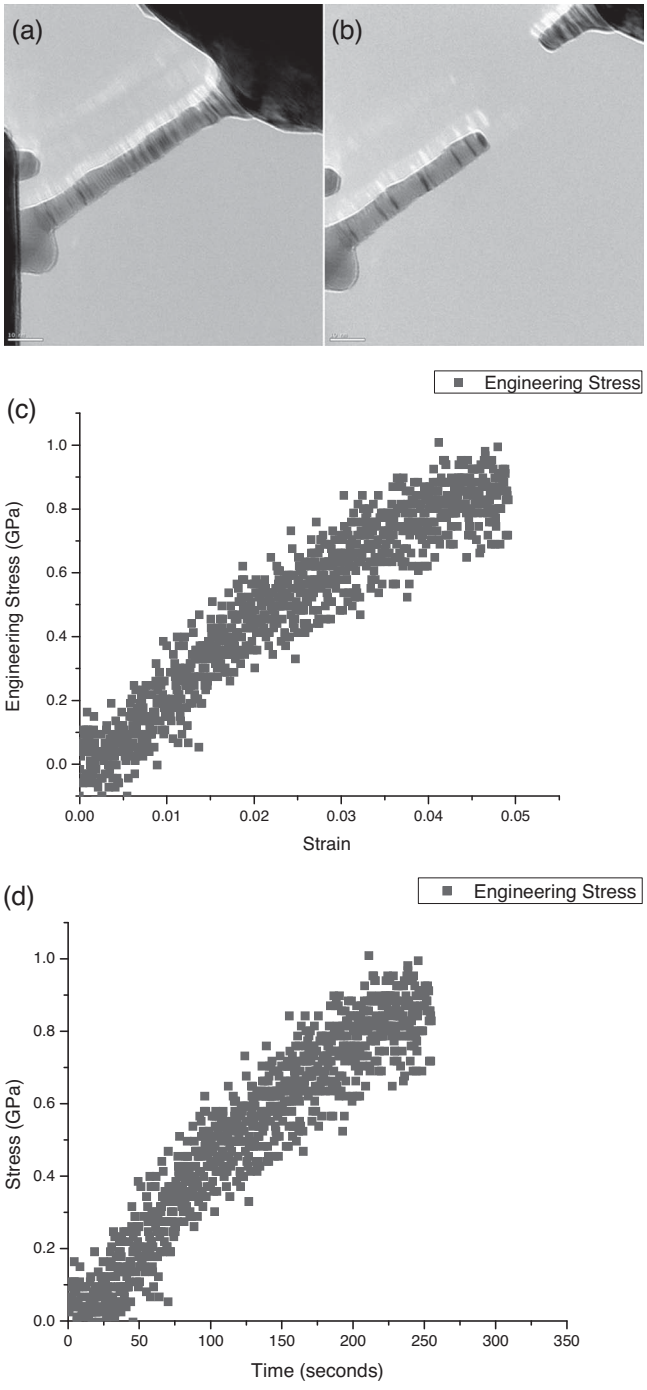

Figure 2. A typical brittle-like fracture of a long nanowire under tension with a low loading rate (~0.1nm/s): a) initial state; b) after breaking (scale bar 10nm); c) corresponding engineering stress-strain curve; d) engineering stress as a function of loading time.

the fracture morphology may change as a function of time, resulting in hard-to-distinguish features under lower TEM imaging magnifications (typical magnifications for most of in situ experiments performed). This could make the last two criteria less reliable. Finally from Table 1, the brittle-like fracture samples had slightly higher engineering fracture strength than

Table 1. Summary of the 22 successful tensile tests for ultrathin gold nanowires.

Sample	Diameter [nm]	Engineering Strength [GPa]	True Strength [GPa]	Fracture Strain
Ductile				
1	8.5	0.598	6.913	0.145
2	7.5	0.774	3.554	0.124
3	9.9	0.822	5.497	0.161
4	7.4	0.889	5.409	0.110
5	9.7	0.654	9.819	0.196
6	5.5	0.813	9.607	0.142
7	10.5	0.960	4.150	0.111
8	10.0	0.620	6.055	0.264
Average	8.6	0.766	6.375	0.156
Brittle-like				
1	14.0	0.641	1.038	0.033
2	10.0	0.892	1.586	0.059
3	7.2	1.008	2.534	0.068
4	9.3	1.860	2.644	0.037
5	7.1	0.875	1.437	0.033
6	9.1	0.625	0.885	0.065
7	10.0	0.827	1.768	0.063
8	10.0	0.552	1.190	0.057
9	7.5	1.550	2.181	0.084
10	8.5	0.601	0.890	0.071
11	6.4	0.939	1.087	0.061
12	10.1	1.034	1.274	0.073
13	7.5	1.000	1.563	0.050
14	10.0	0.600	1.667	0.074
Average	9.0	0.929	1.553	0.059

the ductile fracture samples on average, while samples failed in ductile mode had much higher true fracture strength than the ones failed in brittle-like mode, due to the significant cross-section area reductions during the necking process.

Gold is considered as one of the most ductile metals; at room temperature, fractures with significantly reduced ductility are very rarely reported for gold samples, even at the nanoscale.

Table 2. The criteria to distinguish brittle-like and ductile fractures for ultrathin gold nanowires.

Fracture Modes	Brittle-like	Ductile
Ductility (breaking strain)	AVG 5.9%	AVG 15.6%
Fracture surface morphology	"Cleavage" (flat fracture surface perpendicular to the nanowire axis)	"necking down to a point" (extreme case: atom chain)
Deformation process	limited plastic deformation, sudden fracture	stable necking developments, sustained elongation until final fracture

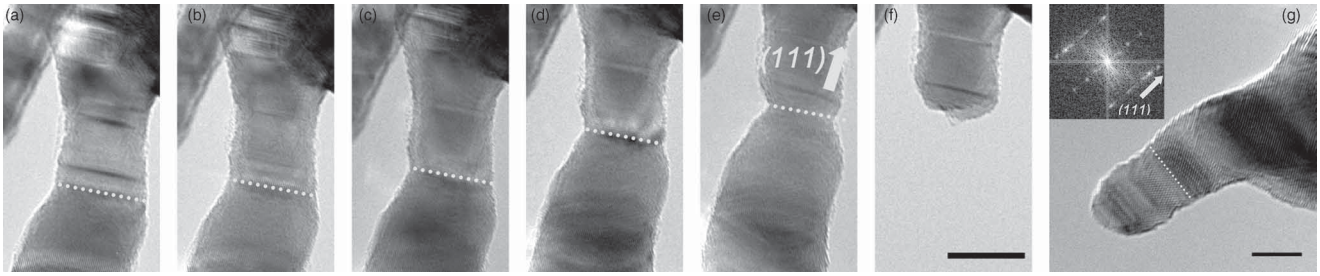

Figure 3. HRTEM tensile test of a short nanowire with twins: a) initial state with three twin boundaries; b) surface non-uniformity near the bottom twin (marked by white dotted line) under tension; c–d) further loading cause stress concentration at the intersection between bottom twin boundary and free surface; e) right before fracture, a groove was formed near the marked twin boundary; f) after fracture along the bottom twin boundary, the top two twin boundaries remained inside the nanowire; g) a nanowire fractured in brittle-like mode, corresponding FFT insert clearly shows the remaining twin structures (all scale bars 5 nm).

One may suggest that higher loading rate could potentially cause this brittle-like fracture for the ultrathin gold nanowire. However, in all 22 successful tensile tests with nanowire diameters ranging from 5–15 nm, 14 of them were fractured in brittle-like mode (see Table 1) and they occurred under various loading rates ranging from 0.1–0.5 nm/s. Loading rates of the same range were applied in the ductile fracture cases. In particular, the specific test shown in Figure 2 was performed at an extremely slow rate of 0.1 nm/s, with the total duration of the experiment reached 250 s (Figure 2d), which is slower than most of the ductile fracture cases. Therefore, the loading rate appears not to be the dominating factor in determining the fracture modes.

Compared to the surface partial dislocation mediated plastic deformation induced ductile fracture of nanoscale metals that has been recently established,[35–38] the unusual brittle-like fracture behavior observed is particularly intriguing as these dimensionally similar nanowire samples were originally all single crystals with the same orientation, and were tested under similar loading rates at room temperature. In order to reveal the underlying mechanism behind this brittle-like fracture, HRTEM analysis was performed for samples failed in brittle-like mode, with the highly magnified image focusing on the broken section. Interestingly, we discovered that there were multiple twin structures near the fracture zone (**Figure 3**) and the boundaries of these twin regions were perpendicular to the nanowire axis. Although the detailed twin structures (i.e., the exact arrangement of several atomic layers at the twin boundary) remain unclear due to the limitation of the atomic resolution, the fracture of nanowire samples appeared to always occur along or near one of these twin regions (Figure 3a–f). Fast Fourier Transformation (FFT) calculation of the sample after fracture (Figure 3g) also confirmed the existence of twin structures in the fractured nanowire. The same link between the observed twin structures on {111} planes of the nanowire samples and the brittle-like fracture mode was confirmed for all 14 samples (Table 1) via high resolution imaging. Moreover, no such twin structures were observed for any of the nanowire samples fractured in ductile mode. This strongly suggested that the twin structure might play a critical role in the brittle-like facture of ultrathin gold nanowires.

Molecular dynamics (MD) simulations were first performed to further assess the role of twinning on subsequent fracture modes. Two different cylindrical Au virtual nanowire samples, one with perfect face-centered-cubic (FCC) structure and another with a sharp interface bounded by an FCC structure and a twin region (colored red in **Figure 4**) at the center simulating the observed twin boundaries, were examined under uniaxial tension between two substrates (see Experimental Section). Here in the twin region, >50% of atoms are distributed in either coherent twin boundaries or stacking faults, both of which are pre-generated via slips perpendicular to the loading (i.e., $\vec{z}$) direction. This twin region is created to mimic the twin structure formed in experiment. In our construction, although some variation of the microstructure in the twin region is allowed, the resultant fracture behavior remains essentially unaltered. The atomistic cross-sectional views of the initial nanowire geometry and final fracture morphology of both samples are shown in Figure 4. The single crystalline FCC nanowire deformed and fractured in a ductile manner with significant elongation and thinning, and sustained large strain (Figure 4a,b). On the other hand, the nanowire with a twin region at the center breaks near the boundary separating the twin region and FCC structure, at a much smaller strain with almost no thinning process (Figure 4c,d). Careful examination of the structural changes during tension and final fracture morphologies of these two samples revealed that the single crystalline nanowire formed two sharp long tips following the substantial necking development; no twin boundaries observed during tension and after failure while substantial dislocation activities were evident. On the other hand, the initially twinned nanowire formed a relatively flat fracture surface, with a few more twin boundaries appearing in the fractured sample (Figure 4d) similar to what has been experimentally observed in Figure 3g. The facture seemed to have initiated near the intersection of the initial twin boundary with the nanowire surface, where surface atom arrangements had been disturbed by the intersection of twin boundary (Figure 3 and **Figure 5**b). In Figure 4e, applied force along nanowire axis direction (F_z) versus elongation (δ) of the nanowires before fracture were plotted, clearly demonstrating that the nanowire with initial twin structure had much less ductility than that of single crystalline nanowire (about 3-4 times differences, correlating well with the experimental results summarized in Table 1). Therefore, the effects of twining on determination of Au nanowire ductility and fracture modes had been verified.

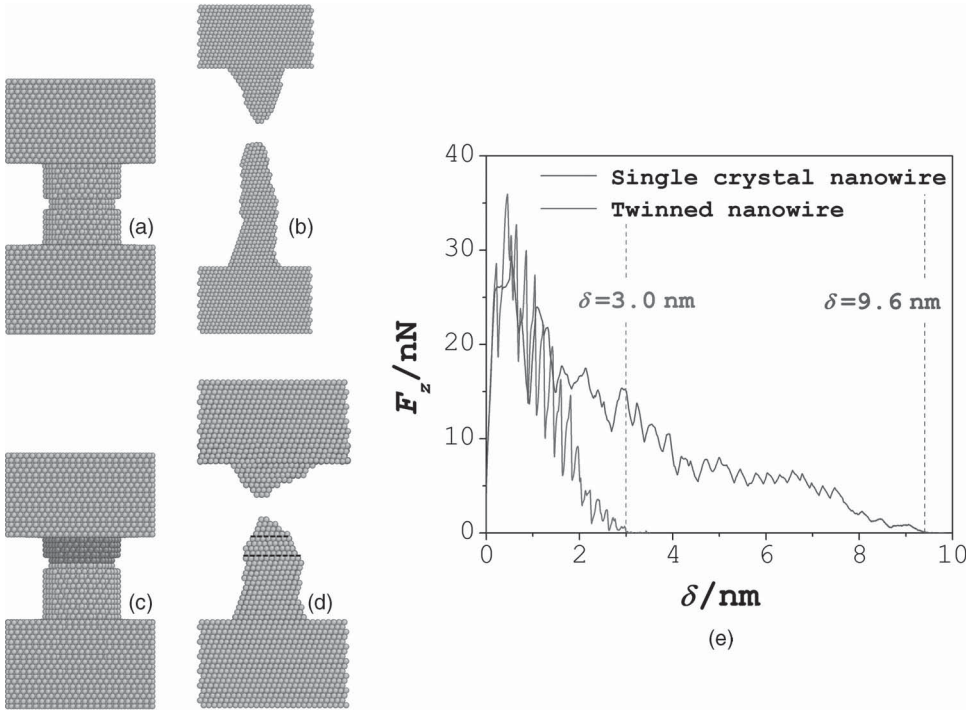

Figure 4. MD simulation of nanowires of comparable dimensions with and without twins in the middle: projection view of a pristine single crystal nanowire without twin a) before loading and b) after fracture; projection view of a nanowire containing a twin structure in the middle (with atoms in the initial twin region coloured in red), c) before loading and d) after fracture; the atomic configurations in (b) and (d) were rotated in order to clearly reveal the remaining twin structures as indicated by black dash lines; e) force versus displacement/elongation curves for both tests.

3. Discussion

Considering the fact that all samples initially have the similar single crystalline <111> structures, it is certainly of interest to examine how these twin structures formed in pristine nanowires. It should be noted that twins can easily form in gold nanowires under various loading conditions as gold has relatively low stacking fault energy.[39] It is possible that those twins may occasionally form during manipulation and sample clamping process. More importantly, we experimentally confirmed that twins could form during tensile loading from the initial single crystalline structure, as shown in Figure 5a,b. Similar type of twin formation in gold nanorod during tensile loading had been also observed experimentally[40] and in computational simulation.[41–43] It is shown that the formation of twins is associated with the stack fault (SF) generation,[40] as well as the collective motion of Shockley partial <112>/6 along {111} slip planes that can transform the structure from FCC to HCP.[41,43]

In Figure 5 as well as in Figure 3, twin boundaries were observed to be perpendicular to the nanowire and loading axis. It is thus a quite logical next step to evaluate the possibility of having a driving force perpendicular to the intended loading direction (along nanowire axial direction) that could result in the formation of the observed twin structures. In all cases where twin formation (e.g., see Figure 2, 3, 5 and Ref. [40]) had occurred, some initial misalignments between nanowire axis and loading directions were always observed. As such misalignment inevitably induced shearing along the transverse planes, it might provide the necessary driving force to promote the nucleation of SF and subsequently the formation of twins.

To validate this possible origin of twin formation due to misalignment induced shearing, we again performed MD simulations. An originally pristine single crystal nanowire oriented along <111> direction was placed under a tensile loading force F. The loading direction is ~11 degree off the wire axis (Figure 5c), introducing a shear component F_t. The corresponding shear stress-strain ($\sigma_t - -\varepsilon_{zt}$) curve was shown in Figure 5d. We observed that once exceeded a critical value ~0.13GPa (well comparable to experiment data taking into consideration of misalignment angle), Shockley partial dislocations were nucleated (see Figure 5e–f) and corresponding load drops were observed (see Figure 5d). It is worth noting that the shear loading component F_t is fairly small compared to the primary tensile loading force, in accordance with small misalignment angles in reality. It is for this reason that no significant load drops were observed in the tensile stress–strain curves of nanowires fractured in brittle-like modes. One thing worth pointing out is that the second partial leads to the formation of an intrinsic stacking fault (Figure 5f), rather than twinning (Figure 5b) as observed in experiment. Nonetheless this discrepancy between simulation and experiment is purely due to MD's inherent limitation in loading rate, and is fairly easy to understand, as explained below. When multiple partial emissions occur, they may either exist in the form of twinning or multiple intrinsic stacking faults (ISFs). Twinning forms when a leading partial is followed by the slip of a twinning partial of the same Burgers vector on the adjacent plane. In this process twinning partial need to overcome the unstable twinning fault

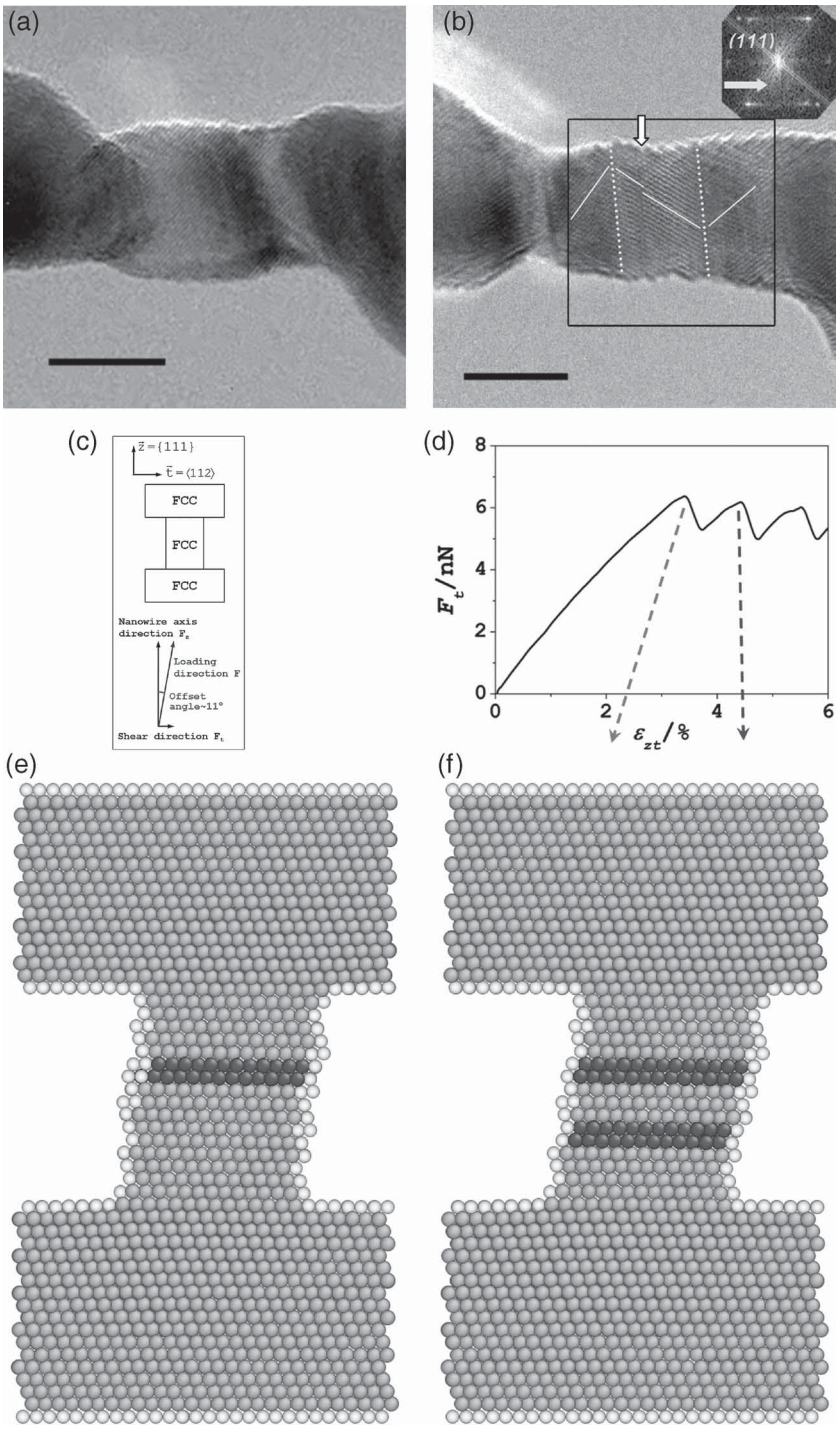

Figure 5. Experimental and computational confirmation of twin formation during tensile loading: a short single crystal nanowire under in situ HRTEM tensile loading, a) before loading and b) after a certain amount deformation with twin formed; In (b), two twin boundaries and a stacking fault (SF) were clearly observed, the inserted FFT confirmed the observed twins were along {111} planes (scale bar 5nm); c) the configuration of shear induced twin formation in MD simulation; d) shear force versus shear strain ε_{zt} plot with corresponding twin formation events (e and f). In e and f, atoms were coloured in yellow representing normal FCC arrangements and coloured in blue representing HCP arrangements.

(~95 mJ/m^2 for current interatomic potential), which is higher than the unstable stacking fault (~89 mJ/m^2 for current interatomic potential). On the other hand, twinning is overall energetically more favorable than multiple ISFs because fewer atoms are left in the fault plane. This competition between twinning and multiple ISFs is well captured by the model developed by D.H. Warner et al.,[44] and depends on the rate of deformation as well as the population of partials. When the nanowire is deformed at the MD loading rate (~1 m/s) and only few partials are emitted, ISFs prevail (e.g., Figure 5f). While for nanowires deformed at the experimental loading rate (~1 nm/s) or abundant partials are emitted, twinning formation is assured. Thus when the sample is subjected to the shear component F_t in experiments (as illustrated in Figure 5c), twinning is indeed expected to occur.

Additionally, considering the fact that misalignments may be unavoidable during the initial stage of tensile tests due to the difficulties associated with sample manipulation and clamping, it is very important to evaluate the magnitude of misalignment that could lead to the observed twin formation and subsequent brittle-like fracture rather than the more classical surface partial dislocation nucleation and propagation mediated ductile fracture. In fact, the initial stage of both conditions was activated by one partial/stacking fault, so we only need to consider those slip systems that result in intrinsic stacking faults (**Figure 6**). From the Thompson Tetrahedrons,[45] we can identify the possible operating slip systems during tensile deformation of the nanowire as following:

1. Twinning partial: $(111)[\bar{1}\bar{1}2]$
2. Non-twinning partials: $(11\bar{1})[112]$, $(\bar{1}11)[211]$ and $(1\bar{1}1)[121]$

Note in Figure 6, only slip systems $(111)[\bar{1}\bar{1}2]$ and $(11\bar{1})[112]$ were shown as they are most relevant if a shear component is induced along $[11\bar{2}]$ direction due to misalignment. By assuming actual loading stress σ and misalignment angle θ, we can calculate the corresponding resolved shear stress on slip systems $(111)[\bar{1}\bar{1}2]$ and $(11\bar{1})[112]$, denoted as τ_T and τ_p, respectively.

$$\tau_T = \sigma \sin\theta \cos\theta$$

$$\tau_p = \sigma \sin(19.47-\theta) \cos(19.47-\theta) - - - 19.47$$

is the angle between [111] and [112] directions

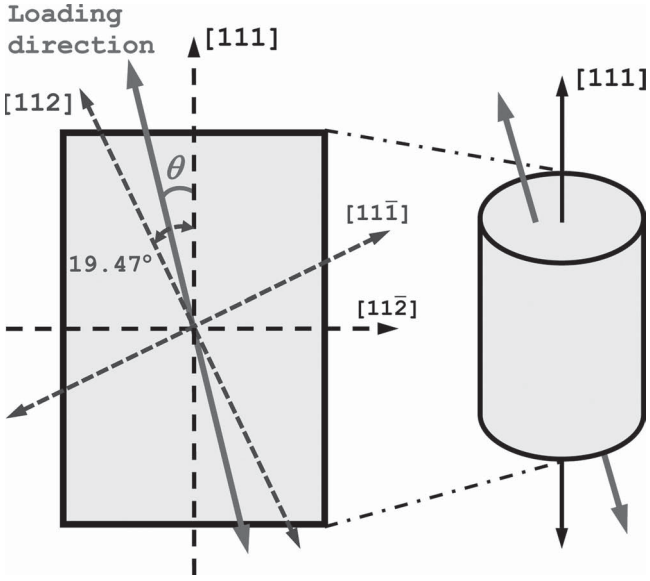

Figure 6. Schematic illustration of loading misalignment with corresponding multiple slip systems for twining partial and normal partial dislocation initiation: the bold red solid line with single-head arrow stands for the loading direction with a misalignment angle theta; and the dotted black (blue) lines with single-head arrow indicate two possible partial dislocation slip systems.

So the criteria of the (111) twin formation prior to the (11$\bar{1}$)[112] partial dislocation slip will be:

$$\tau_T > \tau_p \rightarrow \sigma \sin\theta \cos\theta > \sigma s \text{in}\,(19.47-\theta)\cos(19.47-\theta)$$
$$\rightarrow 4\theta > 38.94 \rightarrow \theta > 9.74\,\text{degree}$$

From this simple calculation, it is clear that when initial misalignment angle θ is small (less than ~9.74°), the shear component τ_T for twinning partial is small. while the shear component for (11$\bar{1}$)[112] non-twinning partial is much larger, resulting in the non-twinning surface partial dislocation nucleation/propagation mediated ductile fracture. However, if the θ is larger than 9.74°, the shear component τ_T for twinning partial will be larger than the shear component for non-twinning partial, resulting in the twin formation and subsequent brittle-like fracture. In the present study, all nanowires failed in ductile fracture mode were initially loaded with <10° misalignment angles and under uni-axial loading geometry once fully stretched, while the nanowires failed in brittle-like fracture mode usually began with fairly large (>15°) misalignment angles. Therefore, this simple criterion based on competition between twin formation and partial dislocation nucleation/propagation as a function of misalignment angle could be used to explain experimentally observed brittle-like and ductile fracture in sub-20 nm gold nanowires.

4. Conclusions

In summary, we have systematically studied the mechanical behaviour of sub-20 nm gold nanowires under tension loading. For nanowires of virtually the same pristine single crystal structure and dimensions, distinct fracture behaviours were observed including both the expected ductile fracture and the unusual brittle-like fracture with low ductility. In the samples that experienced brittle-like fracture, (111) twin structures were found to form during initial loading stage due to small misalignment and the final failure usually occurs along or near one of the twin boundaries. This study provided a comprehensive picture of deformation and fracture mechanisms of ultrathin gold nanowires.

5. Experimental Section

Cold-Welding Assisted Sample Picking-up and Clamping: The individual nanowire was picked up and clamped onto a TEM-AFM holder (NanoFactory Instruments, Sweden), assisted by recently discovered "cold welding" technique.[33] The gold STM tip on one side was first etched further to produce many sharp tips on top of it, and the AFM tip on the other side was also coated with a very thin gold film on which many gold asperities were formed. These nanoscale features served as the clamping spot for cold welding process that securely clamped the ultrathin gold nanowire samples for subsequent tensile testing (also see Supplemental Figure 1).

Stress and Strain Measurement: Instead of relying on direct measurements of image frames in video, we could generate stress–strain curves using the force and displacement output from the TEM–AFM holder equipped with a highly sensitive MEMS–AFM sensor[34] with very high data acquisition rate. The engineering stress was derived from force (F) over the measured initial cross-section area. The engineering strain was obtained using the elongation of the nanowire sample between clamping point over the initial gauge length L_0, $\varepsilon = \Delta D/L_0$. Since the direct displacement reading was the STM withdrawing distance (D_S), the actually elongation of nanowire ΔD should equal the STM withdrawing displacement minus the AFM cantilever deflection distance (D_A, could be obtained by F/k, where k is the spring constant of the cantilever and F could be obtained directly), $\Delta D = D_S - D_A$. It should be noted that, both D_S and D_A were carefully calibrated based on the actual video frames of individual tensile experiment.

Molecular Dynamics (MD) Simulation: Nanowire samples are initially of the same crystalline orientation (except for the twin region shown in Figure 4c), as well as of the same vertical and radial dimensions (i.e., L = 4.2 nm and D = 3.5 nm) in cylindrical shape with each being separately sandwiched between two substrates. A circular notch was created initially in the nanowire either at the middle position or at the twin boundary (Figure 4a and c), to resemble the surface non-uniformity observed in experiments (Figure 3). This notch also served as the position for initial deformation to occur. In Figure 4c atoms in twin region were coloured in red with other atoms coloured in orange, while in Figure 5e–f atoms were coloured via the local order parameter proposed by Steinhardt et al.[46]

The simulations were performed in a NVT ensemble with the temperature maintained at 300K using a Nosé–Hoover thermostat.[47] During the simulations, the top and bottom substrates were brought apart at a constant speed of v_z = 0.2 m/s, stretching the nanowire clamped in between until final fracture. The inter-atomic potential employed in the present study to describe the interactions between atoms is the embedded-atom method (EAM)[48,49] potential for Au developed by Cai and Ye.[50]

Supporting Information

Supporting Information is available from the Wiley Online Library or from the author.

Acknowledgements

The authors acknowledge the financial support provided by the Air Force Office of Sponsored Research (AFOSR) YIP award FA9550-09-

1-0084 and by NSF grant ECCS-0702766. This work was performed, in part, at the Center for Integrated Nanotechnologies, a U.S. Department of Energy, Office of Basic Energy Sciences user facility at Los Alamos National Laboratory (Contract DE-AC52-06NA25396) and Sandia National Laboratories (Contract DE-AC04-94AL85000). Sandia National Laboratories is a multi-program laboratory operated by Sandia Corporation, a wholly owned subsidiary of Lockheed Martin company, for the U.S. Department of Energy's National Nuclear Security Administration under contract DE-AC04-94AL85000.

Received: May 28, 2011
Revised: July 5, 2011
Published online:

[1] Y. Xiong, Z. Liu, X. Zhang, *Appl. Phys. Lett.* **2009**, *94*, 203108.
[2] L. Cademartiri, G. A. Ozin, *Adv. Mater.* **2009**, *21*, 1013.
[3] C. Wang, Y. Hu, C. M. Lieber, S. Sun, *J. Am. Chem. Soc.* **2008**, *130*, 8902.
[4] Z. Huo, C. Tsung, W. Huang, X. Zhang, P. Yang, *Nano Lett.* **2008**, *8*, 2041.
[5] X. Lu, M. S. Yavuz, H. Tuan, B. A. Kogel, Y. Xia, *J. Am. Chem. Soc.* **2008**, *130*, 8900.
[6] H. Feng, Y. Yang, Y. You, G. Li, J. Guo, T. Yu, Z. Shen, T. Wu, B. Xing, *Chem. Commun.* **2009**, 1984.
[7] B. H. Hong, S. C. Bae, C. W. Lee, S. Jeong, K. S. Kim, *Science* **2001**, *294*, 348.
[8] J. J. Zhao, C. L. Buia, J. Han, J. P. Lu, *Nanotechnology* **2003**, *14*, 501.
[9] Z. Y. Tang, N. A. Kotov, *Adv. Mater.* **2005**, *17*, 951.
[10] J. W. Liu, J. H. Zhu, C. L. Zhang, H. W. Liang, S. H. Yu, *J. Am. Chem. Soc.* **2010**, *132*, 8945.
[11] H. W. Liang, S. Liu, J. Y. Gong, S. B. Wang, L. Wang, S. H. Yu, *Adv. Mater.* **2009**, *21*, 1850.
[12] X. Teng, W. Han, W. Ku, M. Hucker, *Angew. Chem. Int. Ed.* **2008**, *47*, 2055.
[13] S. Yang, F. Hong, L. Wang, S. Guo, X. Song, B. Ding, Z. Yang, *J. Phys. Chem. C* **2010**, *114*, 203.
[14] W. Lu, C. M. Lieber, *Nat. Mater.* **2007**, *6*, 841.
[15] B. Wu, A. Heidelberg, J. J. Boland, *Nat. Mater.* **2005**, *4*, 525.
[16] Y. Zhu, H. D. Espinosa, *Proc. Natl. Acad. Sci. USA* **2005**, *102*, 14503.
[17] Y. Lu, Y. Ganesan, J. Lou, *Experimental Mechanics* **2010**, *50*, 47.
[18] Y. Ganesan, Y. Lu, C. Peng, H. Lu, R. Ballarini, J. Lou, *J. Microelectromech. Syst.* **2010**, *19*, 675.
[19] D. Zhang, J. M. Breguet, R. Clavel, L. Philippe, I. Utke, J. Michler, *Nanotechnology* **2009**, *20*, 365706.
[20] G. Richter, K. Hillerich, D. S. Gianola, R. Mönig, O. Kraft, C. A. Volkert, *Nano Lett.* **2009**, *9*, 3048.
[21] J. R. Greer, W. D. Nix, *Phys. Rev. B* **2006**, *73*, 245410.
[22] Z. W. Shan, R. K. Mishra, S. A. Syed Asif, O. L. Warren, A. M. Minor, *Nat. Mater.* **2008**, *7*, 115.
[23] M. D. Uchic, D. M. Dimiduk, J. N. Florando, W. D. Nix, *Science* **2004**, *305*, 986.
[24] D. Jang, J. R. Greer, *Nat. Mater.* **2010**, *9*, 215.
[25] S. Buzzi, M. Dietiker, K. Kunze, R. Spolenak, J. F. Loffler, *Philosoph. Mag.* **2009**, *89*, 869.
[26] T. Kizuka, *Phys. Rev. B* **1998**, *57*, 11158.
[27] G. Rubio, S. R. Bahn, N. Agrait, K. W. Jacobsen, S. Vieira, *Phys. Rev. Lett.* **2001**, *87*, 026101.
[28] Y. Kondo, K. Takayanagi, *Phys. Rev. Lett.* **1997**, *79*, 3455.
[29] B. L. Boyce, J. Y. Huang, D. C. Miller, M. S. Kennedy, *JOM* **2010**, *62*, 62–63.
[30] H. Hirayama, Y. Kawamoto, Y. Ohshima, K. Takayanagi, *App. Phys. Lett.* **2001**, *79*, 1169–1171.
[31] L. X. Dong, X. Y. Tao, L. Zhang, X. B. Zhang, B. J. Nelson, *Nano Lett.* **2007**, *7*, 58.
[32] D. Hyman, M. Mehregany, *IEEE Trans. Compon. Packag. Technol.* **1999**, *22*, 357.
[33] Y. Lu, J. Y. Huang, C. Wang, S. Sun, J. Lou, *Nature Nanotech.* **2010**, *5*, 218.
[34] A. Nafari, D. Karlen, C. Rusu, K. Svensson, H. Olin, P. Enoksson, *J. Microelectromech. Syst.* **2008**, *17*, 328.
[35] E. Rabkin, D. J. Srolovitz, *Nano Lett.* **2007**, *7*, 101.
[36] T. Zhu, J. Li, A. Samanta, A. Leach, K. Gall, *Phys. Rev. Lett.* **2008**, *100*, 025502.
[37] Y. Lu, Ph.D Thesis, In Situ Quantitative Mechanical Characterization and Integration of One Dimensional Metallic Nanostructures, Rice University, **2011**.
[38] H. Zheng, A. Cao, C. R. Weinberger, J. Y. Huang, K. Du, J. Wang, Y. Ma, Y. Xia, S. X. Mao, *Nat. Comm.* **2010**, *1*, 144.
[39] C. Deng, F. Sansoz, *Nano Lett.* **2009**, *9*, 1517.
[40] M. J. Lagos, F. Sato, D. S. Galvao, D. Ugarte, *Phys. Rev. Lett.* **2011**, *106*, 055501.
[41] J. Song, D. J. Srolovitz, *Scripta Mater.* **2007**, *57*, 885.
[42] J. Song, D. J. Srolovitz, *J. Appl. Phys.* **2008**, *104*, 124312.
[43] J. Song, D. J. Srolovitz, *Acta Mater.* **2007**, *55*, 4759.
[44] D. H. Warner, W. A. Curtin, S. Qu, *Nat. Mater.* **2007**, *6*, 1004.
[45] N. Thompson, *Proc. Phys. Soc. B* **1953**, *66*, 481.
[46] P. J. Steinhardt, D. R. Nelson, M. Ronchetti, *Phys. Rev. B* **1983**, *28*, 784.
[47] S. Nose, *J. Chem. Phys.* **1984**, *81*, 511.
[48] M. S. Daw, M. I. Baskes, *Phys. Rev. B* **1984**, *29*, 6443.
[49] S. M. Foiles, M. I. Baskes, M. S. Daw, *Phys. Rev. B* **1986**, *33*, 7983.
[50] J. Cai, Y. Y. Ye, *Phys. Rev. B* **1996**, *54*, 8398.